Predicting quadrupole relaxation enhancement peaks in proton R_1-NMRD profiles in solid Bi-aryl compounds from NQR parameters

Christian Gösweiner, Danuta Kruk, Evrim Umut, Elzbieta Masiewicz, Markus Bödenler & Hermann Scharfetter

Taylor & Francis
Taylor & Francis Group

🔓 OPEN ACCESS   Check for updates

Predicting quadrupole relaxation enhancement peaks in proton R_1-NMRD profiles in solid Bi-aryl compounds from NQR parameters

Christian Gösweiner [a], Danuta Kruk [b], Evrim Umut[b], Elzbieta Masiewicz[b], Markus Bödenler[a] and Hermann Scharfetter[a]

[a]Institute of Medical Engineering, Graz, Austria; [b]Faculty of Mathematics and Computer Science, University of Warmia and Mazury in Olsztyn, Olsztyn, Poland

ABSTRACT

We propose a simple method to calculate and predict quadrupole relaxation enhancement (QRE) features in the spin-lattice nuclear magnetic relaxation dispersion (R_1-NMRD) profile of protons (^{1}H) in solids. The only requirement is the knowledge of the nuclear quadrupole resonance (NQR) parameters of the quadrupole nuclei in a molecule. These NQR parameters – the quadrupole coupling constant Q_{cc} and the asymmetry parameter η – can be determined by NQR spectroscopy or using quantum chemistry calculations. As there is an increasing interest in using molecules producing high field QRE features as, e.g. for contrast enhancing agents in magnetic resonance imaging, the experimental efforts of seeking for suitable compounds can be reduced by pre-selecting molecules via calculations. Also, the method can be used to extract NQR parameter, and thus structural information, from R_1-NMRD profiles showing QRE features. In this article, we describe the calculation procedure and present examples of comparing the result to experimental R_1-NMRD data of two different solid ^{209}Bi-aryl compounds.
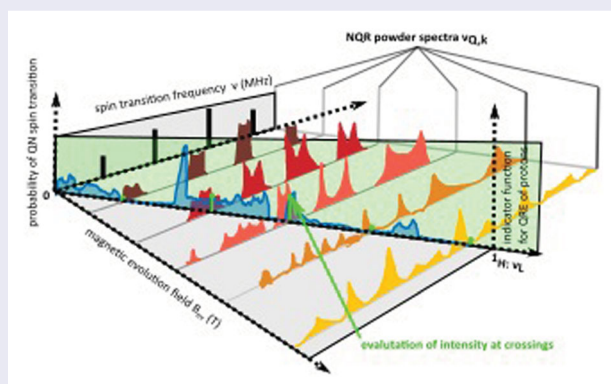
1. Introduction

An application of nuclear magnetic resonance (NMR), forming a field of research by its own, is the measurement of spin-lattice relaxation rates R_1 of nuclear spins. Experiments can be performed on a great variety of materials from condensed matter to liquids. As one is typically interested in molecular motions, such measurements are done temperature and/or field dependent by means of NMR field cycling (FC) relaxometry [1]. This method allows to study $R_1(\nu_L)$ of protons on a broad band Larmor frequency scale ν_L which is achieved by

stepping the external magnetic field value B_{ev} (evolution field) applied to the sample at different cycles during a dispersion measurement. The experimental procedure uses an elaborate way of cycling the magnetic field in a sequence for enabling polarisation, evolution and detection of a nuclear spin ensemble. The evolution field can typically be varied to create proton Larmor frequencies from as low as 10 kHz to about 40 MHz. The experiments presented later in this article, however, are conducted between 20 and 128 MHz by the use of an additional superconducting 3 T magnet [2]. An early detailed

description of the method can be found in the work of F. Noack [3], a more recent review is given in reference [1]. FC-NMR relaxometry nowadays is a standard analysis method and is applied to a wide range of research fields as, e.g. ionic crystals [4], liquid crystals [5], lipids [6], polymer dynamics [7], porous media [8] or, as formulated quite generally in another review [9], to *molecular dynamics in complex media*. The resulting measurements of the frequency dependence of R_1 are often referred to as nuclear magnetic relaxation dispersion (NMRD) profile. A method for gaining insight into molecular dynamics from analysing NMRD profiles is, e.g. the Redfield relaxation theory [10].

However, not only dynamical properties but also structural information from solids is accessible from NMRD measurements. The quadrupole relaxation enhancement (QRE, [11–15]) effect can create pronounced and prominent features (peaks) in the R_1-NMRD profile, depending on the type of quadrupole nuclei (QN, $I > 1/2$) and structure of their electronic surrounding. This so-called QRE peaks (also called quadrupolar dips in case of a $T_1 = 1/R_1$ dispersion representation) emerge due to a magnetisation transfer from the protons to nearby (only several Å) QN via magnetic dipole dipole (D–D) coupling which is manifested in an increase of the relaxation rate R_1 of the proton spins. The effect is frequency (magnetic field) dependent, because QRE can only occur where both the transition frequencies ν_L of the protons (their Larmor frequency) and ν_Q of a coupled pool of quadrupole nuclei match (see Figure 1). One of the first articles demonstrating this effect is dealing with powdery polyvinylchloride containing ^{35}Cl and ^{37}Cl nuclei ($I = 3/2$) [12]. Also, studies on solids containing ^{14}N [16, 17] were reported. Cases
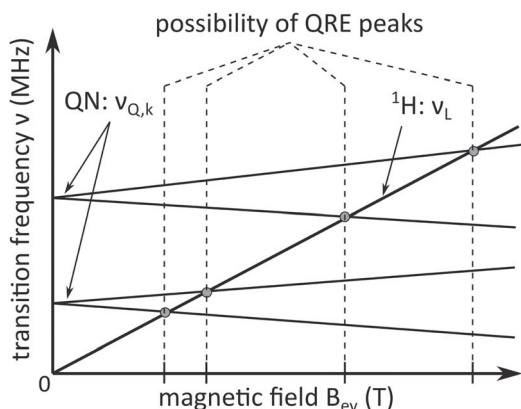
were presented, where ^{14}N ($I = 1$) nuclei produce QRE peaks in the NMRD profile of biological systems, e.g. proteins in muscles [18, 19]. Lurie *et al.* [20] have utilised this effect for magnetic resonance imaging (MRI) and could demonstrate a contrast enhancement in $T_1 = 1/R_1$ weighted images using a special field cycling MRI systems at low magnetic field strengths (< 200 mT). Field cycling MRI has also been successfully demonstrated at clinical field strengths of 1.5 T [21–23] and 3 T [24]. Recently, strong and pronounced QRE peaks have been observed in NMRD measurements of different Bi-aryl compounds [2]. The experimental data of this article will be used to evaluate the herein presented simulation.

Aim of this work is to predict the location of QRE peaks in proton R_1-NMRD profiles of solids from the nuclear quadrupole resonance (NQR) parameters of the QRE-active nuclei by calculating NQR transition probabilities. As we do not directly include relaxation processes, the approach is fairly simple to calculate and gives, as is shown later, reliable results. This is especially favourable when considering the increasing interest in QN compounds creating QRE peaks in proton R_1-NMRD profiles at high fields (e.g. 3 T) to use them as MRI contrast agents [25] while the measurements of such is not yet straightforward and connected with technical challenges. Also, the availability of such systems is not yet very high. The NQR parameters on the contrary are accessible with NQR spectrometers working in the radio frequency regime and to some degree also through quantum chemistry (QC) calculations. Of course, the approach can also be used for the other way round: determining NQR parameters from NMRD profiles showing QRE peaks which could be used to double check NQR results or to support the determination of NQR parameters where NQR spectroscopy is problematic.

The central idea can be summarised by formulating four assumptions:

Assumption (1): As in solid powders, the nuclei cannot rotate freely their energy level structure is essentially static and determines the NQR powder spectra $\nu_Q(B_{ev})$ in the presence of an external magnetic field by applying the unperturbed total Hamiltonian as a sum of quadrupole and Zeeman Hamiltonian. From that, the transition probability $p_Q(B_{ev})$ can be calculated by summing up all contributions over all orientations of the crystallites.

Assumption (2): QRE can only occur at magnetic fields B_{ev} at which $\nu_L(B_{ev})$ matches a QN transition frequency $\nu_Q(B_{ev})$.

Assumption (3) states that the QRE amplitude at B_{ev} depends on the joint transitions probability between eigenstates of the spin system of the QN -^1H pair mediated by D–D coupling. As we neglect the proton

Figure 1. Scheme of the nuclear spin transition frequency for a proton ν_L and a QN ν_Q with $I = 5/2$ versus the magnetic evolution field. At the B_{ev} field positions of the level crossings, QRE features can be expected in case that there is a D–D coupling present between QN and proton originating from spin fluctuations due to molecular motions.

relaxation, the sole QN transitions probability $p_Q(B_{ev})$ is considered. This has the consequence that the QRE amplitudes will not be reproduced completely correct.

Assumption (4) proposes that the relaxation of NQR transitions due to perturbations of the QN energy level structure (which acts as the mechanism in the QRE process for dissipating the magnetisation to the lattice) can be regarded as small and enters the calculation only phenomenological by the assumption of a certain linewidth for zero field transitions.

2. Theory

2.1. The calculation procedure

Details of how to calculate the NQR powder spectrum will be the matter of the following sections, but to understand the calculation procedure, one has to know that a QN can already exhibit excitable spin transitions $\nu_{Q,k}$ at zero magnetic field [26]. Depending on its nuclear spin quantum number I, one can observe – in case of half integer spins – $I + 1/2 - 1$ transitions k. As ν_L is given by the product of the proton's gyromagnetic ratio γ_p times, the applied field B_{ev} in qualitatively the same way as the splitting of quadrupole transitions is given by γ_{QN} times B_{ev}, the only determinant of the frequency locations of the transition crossings are the pure quadrupole

transition frequencies of the QN at zero magnetic field (see Figure 1). These are the result of an electrical interaction between the electric field gradient (EFG) at the nucleus of interest and its quadrupole moment Q being present in the QN containing molecule.

Keeping this in mind, the calculation procedure can best be explained by an extension of Figure 1 towards a more general case where the EFG is not aligned with B_{ev} but randomly uniformly distributed, thus leading to a powder spectrum at each B_{ev} (see Figure 2). Also, the intensity of the NQR powder spectrum is included. Again, the nuclear spin transition frequencies of a proton and a QN in the presence of a magnetic evolution field B_{ev} are plotted in the transversal plane. On the z-axis additionally, the intensity of the NQR powder spectrum is drawn. So, Figure 2 shows the spectral NQR intensity as a function of frequency in dependence on the magnetic field. In particular, six selected NQR spectra are drawn and labelled with colours from dark red to yellow, the brightness indicating the increasing B_{ev}. The oblique plane is aligned with the proton Larmor frequency ν_L and thus acts as an indicator function which cuts out the quadrupole transition probability exactly at the corresponding crossover points, as indicated exemplary by the vertical light green lines ('evaluation points'). The resulting pattern along this indicator plane is used for predicting the QRE transition probability and thus those bands where QRE most likely can be expected. As it does not
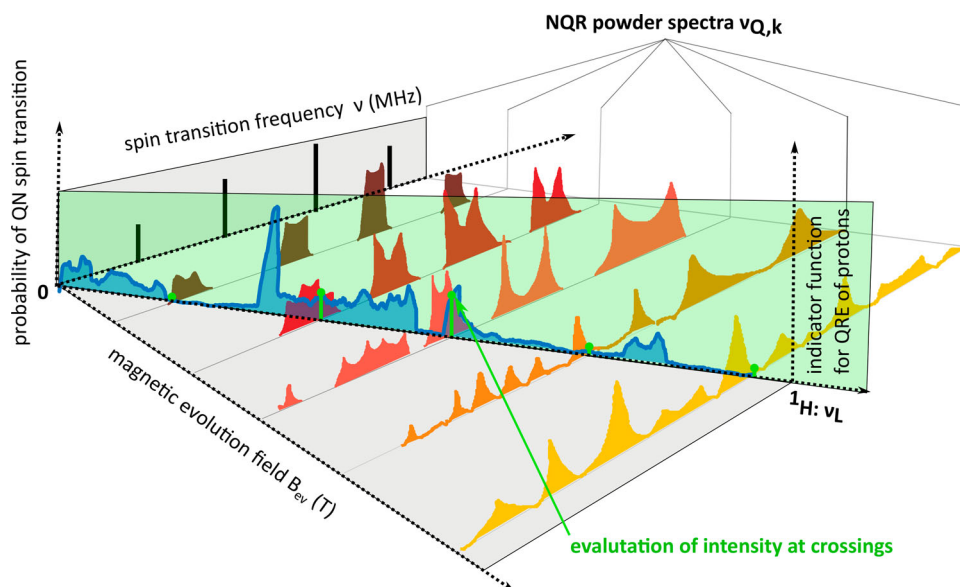
Figure 2. Scheme to illustrate the calculation procedure for predicting QRE peak positions in NMRD measurements. The x–y plane of the 3D plot is spanned by the spin transition frequency versus the magnetic field B_{ev} which is applied to a proton and a QN. The z-axis gives the intensity of the NQR powder spectrum which depends on the QN spin transition probability p_Q. When following the proton Larmor frequency ν_L along the x–y plane, the NQR spectrum intensity can be evaluated at a set of points along the magnetic evolution field. Some evaluation positions, which correspond to the transition crossings, are marked with vertical solid lines on the transparent, vertical plane that follows ν_L (in green colour). The thereby generated intensity profile drawn in that plane (in blue) gives an estimate for the probability of a QRE feature in an R_1-NMRD profile of slowly rotating or static (in solids) systems (Colour online, B&W in print).

account for lineshapes or spectral densities of the D–D fluctuations, it must not be interpreted quantitatively, i.e. in terms of QRE strength.

2.2. NQR powder spectrum

The required theory in order to obtain the quadrupole transition frequencies ν_Q and their expectable NQRS intensities $I_{\text{NQR}}(\nu_Q)$ in the presence of an external static magnetic field B_0 is well described in references [26–28] and will be adapted and summarised in the following section.

The interaction of nuclei exhibiting a quadrupole moment Q (for $I > 1/2$) with an electric field gradient (EFG, $V_{ij} = \partial^2 V / \partial x_i \partial x_j$) resulting from surrounding binding electrons forming the electrostatic potential V gives rise to discrete energy levels of the nuclear spin. A nucleus with, e.g. spin number $I = 5/2$, has $2I+1 = 6$ energy levels denoted with $m = -I \cdots + I$.

The interaction can be fully described by just two parameters: the quadrupole coupling constant Q_{cc} and the asymmetry parameter η which appear in the pure NQR Hamiltonian $\widehat{H}_Q(I)$ in the laboratory frame (LAB):

$$\widehat{H}_Q(I)^{\text{LAB}} = \frac{Q_{cc}}{I(2I-1)} \sum_{m=-2}^{2} (-1)^m T_m^{(2)} V_{-m}^{(2)\text{LAB}} \quad (1a)$$

$$T_0^{(2)}(I) = \frac{1}{2}(3\widehat{I}_z^2 - I(I+1))$$

$$T_{\pm 1}^{(2)}(I) = \frac{\sqrt{6}}{4}(\widehat{I}_z\widehat{I}_\pm + \widehat{I}_\pm\widehat{I}_z) \quad (1b)$$

$$T_{\pm 2}^{(2)}(I) = \frac{\sqrt{6}}{4}\widehat{I}_\pm^2$$

$Q_{cc} = e^2qQ/\hbar$ is made up of the product of the EFG strength eq and the quadrupole contribution eQ with the quadrupole moment Q. The asymmetry parameter $\eta = (V_{xx} - V_{yy})/V_{zz}$ is a measure for the deviation of the EFG from cylinder symmetry. The $\widehat{I}$'s denote the usual spin angular momentum operators.

As we are applying an external static magnetic field, the Zeeman Hamiltonian $\widehat{H}_Z(I)$ has to be added to the total Hamiltonian $\widehat{H}_0(I)(\Omega)$:

$$\widehat{H}_0(I)(\Omega) = \widehat{H}_Z(I) + \widehat{H}_Q(I)(\Omega). \quad (2a)$$

$$\widehat{H}_Z(I) = -\gamma_{\text{QN}} \overrightarrow{B}_{\text{ev}} \cdot \overrightarrow{I} \quad (2b)$$

$\widehat{H}_Z(I)$ introduces an angle dependency $\Omega = (\alpha, \beta, \gamma)$ between the direction of the EFG and the applied magnetic field $\overrightarrow{B}_{\text{ev}}$. γ_{QN} is the gyromagnetic ratio of the quadrupole nucleus under investigation.

In order to account for the required rotation into the same coordinate system (LAB), the spatial tensor operators $V_m^{(2)}$ have to be written in the following form [28]:

$$V_0^{(2)\text{LAB}} = \frac{1}{2}\left[\frac{(3\cos^2\beta - 1)}{2} + \frac{\eta}{4}\sin^2\beta(e^{-2i\gamma} + e^{-2i\gamma})\right]$$

$$V_{\pm 1}^{(2)\text{LAB}} = \frac{1}{2}\left[\mp\sqrt{\frac{3}{8}}\sin 2\beta e^{\pm i\alpha}\right.$$

$$+ \frac{\eta}{\sqrt{6}}\left(-\frac{1\mp\cos\beta}{2}\sin\beta e^{\pm i(\alpha\mp 2\gamma)}\right.$$

$$\left.\left.+ \frac{1\mp\cos\beta}{2}\sin\beta e^{i(\pm\alpha+2\gamma)}\right)\right]$$

$$V_{\pm 2}^{(2)\text{LAB}} = \frac{1}{2}\left[\sqrt{\frac{3}{8}}\sin^2\beta e^{\pm 2i\alpha}\right.$$

$$+ \frac{\eta}{\sqrt{6}}\left(\frac{(1\mp\cos\beta)^2}{4}e^{\pm 2i(\alpha\mp\gamma)}\right.$$

$$\left.\left.+ \frac{(1\pm\cos\beta)^2}{4}e^{2i(\pm\alpha+\gamma)}\right)\right]$$

$$(3)$$

To finally obtain the transition frequencies ν_Q, the total Hamiltonian from (2a) is being diagonalised numerically and we end up with the energy levels E_α of the spin system with respect to the eigenfunctions $|\Psi_\alpha(\Omega)\rangle = \sum_{m=-1}^{2I+1} a_{\alpha,m}(\Omega)|I, m\rangle$, where $\{|I, m\rangle\}$ is the orthonormal Zeeman basis, in short, written as $\{|m\rangle\}$. The angle-dependent NQR transition frequencies $\nu_Q(\Omega)$ at an external magnetic field B_{ev} can be expressed by the difference between two energy levels E:

$$\nu_Q(\Omega, B_{\text{ev}}) = E_\alpha - E_\beta = \langle\Psi_\alpha(\Omega)|\widehat{H}_0(I)(\Omega)|\Psi_\alpha(\Omega)\rangle$$

$$- \langle\Psi_\beta(\Omega)|\widehat{H}_0(I)(\Omega)|\Psi_\beta(\Omega)\rangle \quad (4)$$

2.3. Intensity of the NQR powder spectrum

A NQR experiment can be performed by exciting a QN spin transition with an oscillating magnetic field with amplitude $\overrightarrow{B}_{\text{RF}}$ in an arbitrary direction (x, y, z) at angular frequency ω_{RF} and phase ϕ_{RF} described by the RF-Hamiltonian [28]

$$\widehat{H}_{\text{RF}} = -\gamma_{\text{QN}}\overrightarrow{B}_{\text{RF}} \cdot \overrightarrow{I} \cdot \cos(\omega_{\text{RF}}t - \phi_{\text{RF}}) \quad (5)$$

The expected relative intensity for each transition $\nu_Q(\Omega)$ when an evolution field B_{ev} is applied can be written as a product of the quantum mechanical transition probability p_{NQR} times the Boltzmann population difference p_T

of the energy levels at the ensemble temperature T:

$$I_{\mathrm{NQR}}(\nu_Q)(\Omega, B_{\mathrm{ev}}) = p_{\mathrm{NQR}} \cdot p_T$$

$$= |\langle \Psi_\alpha(\Omega)|\widehat{H}_{\mathrm{RF}}|\Psi_\beta(\Omega)\rangle|^2 \cdot \frac{e^{(E_\alpha - E_\beta)/k_B T}}{\sum_{i,j} e^{(E_i - E_j)/k_B T}} \quad (6)$$

where k_B is Boltzmann's constant.

To describe a powder spectrum, the frequencies from Equation (4) and their corresponding intensities (Equation (6)) are being evaluated for a set of N random, uniformly distributed angles Ω on a sphere. Then, each intensity value is assumed to represent a Lorentzian peak with an experimentally determined and constant full width at half maximum (FWHM) derived from zero-field NQR measurements. The Lorentzians with $\gamma = FWHM/2$ are then summed up and averaged according to Equation (7).

$$\bar{I}_{\mathrm{NQR}}(\nu_Q)(B_{\mathrm{ev}}) = \sum_\Omega \left[\frac{I_{\mathrm{NQR}}(\nu_Q)(\Omega, B_{\mathrm{ev}})}{1 + (\nu - \nu_Q(\Omega, B_{\mathrm{ev}}))/\gamma} \right] \bigg/ N \quad (7)$$

In Figure 3, the result of such a procedure is demonstrated for triphenylbismuth in a field B_{ev} of 100 mT. The clouds of single grey stars in the background represent the intensity values for each of the randomly chosen angles Ω on a unit sphere according to Equation (6), the blue solid line is the average according to (7) and shows the calculated NQR spectrum at a field strength of 100 mT. The noisy, oscillatory shape of the spectrum is a result of the random input parameters and the frequency step size. For higher number of angles N and a smaller step size, the lineshape of the spectrum becomes smoother.

2.4. The relevant intensity of the NQR powder spectrum

The intensity $\bar{I}_{\mathrm{NQR}}(\nu_Q)(B_{\mathrm{ev}})$ as described in Section 2.3 is the intensity that can be expected from a measurement using a NQR spectrometer. Typically, $\widehat{H}_{\mathrm{RF}}$ in Equation (6) reduces to $\widehat{I}_x$, when the RF field oscillates perpendicular to the applied magnetic field. But we are interested in the QRE effect which is manifested in magnetic field selective R_1-relaxation enhancement features in NMRD profile measurements. In this case, two spin species and their corresponding transitions are involved. To figure out what are the allowed transitions, we should have a
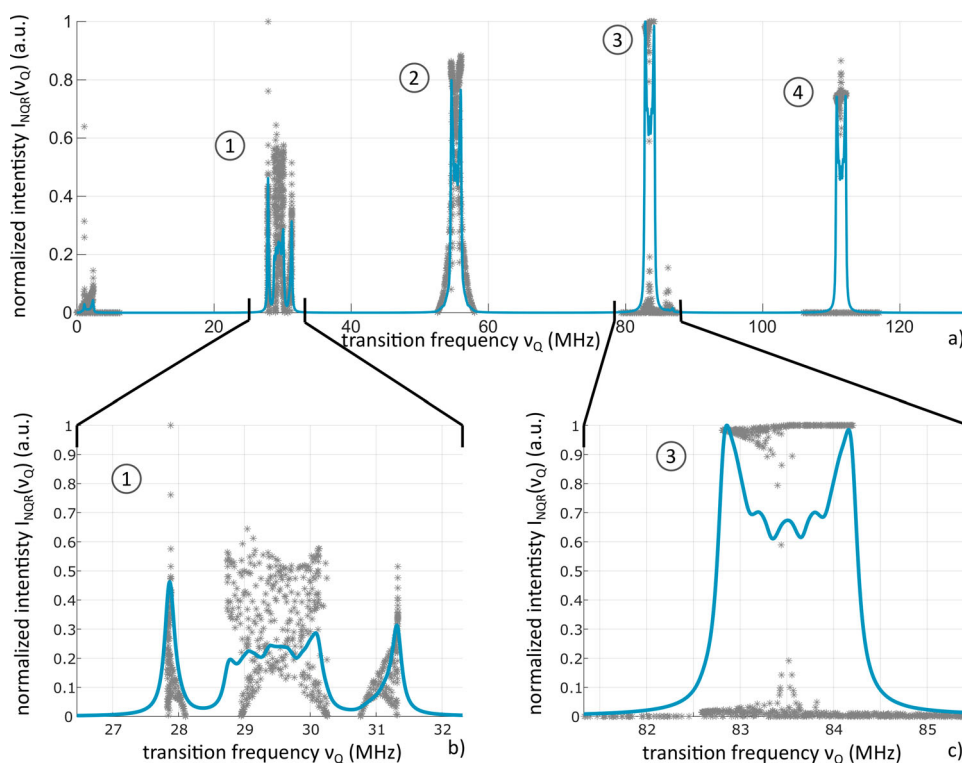

Figure 3. Simulated NQR powder spectrum at an external magnetic field of 100 mT for triphenylbismuth according to Equation (7). The grey dots in the background correspond to the result of Equation (6) evaluated for a single angle Ω. The solid line (blue) gives the normalised summation of all stars in the background according to Equation (7). Panel (a) shows the whole spectrum from 0 to 120 MHz. Panels (b) and (c) zoom into two selected bands which show the splitting of transition 1 and 3, respectively. While transition 3 shows a typical Pake-pattern, the low-frequency pattern corresponding to transition 1 is comparatively complex. The reason for this shape has been described elsewhere [26]. Input parameters for triphenylbismuth from reference [25]: $Q_{cc} = 668.87e6$ MHz, $\eta = 0.08$, $I = 9/2$, $\gamma_{Bi} = 6.95$ MHz/T, FWHM of signal intensity $= 40$ kHz. $N = 200$ (Colour online, B&W in print).

closer look at what is happening at the level crossings: Assuming that the proton with $I = 1/2$ in a magnetic field is performing a transition from $|-1/2\rangle$ to $|+1/2\rangle$ during spin-lattice relaxation, the angular momentum changes by $\Delta m = +1$. To act like an energy sink and take over the corresponding magnetisation, the QN has to perform a spin transition with the same energy by $\Delta m = -1$ (e.g. $|-3/2\rangle$ to $|-5/2\rangle$), which corresponds to an excitation. The operator that can mediate such a transition within the QN energy level system is the lowering operator $\widehat{I}_-$. In that case, the intensity of NQR transitions available for the protons for performing QRE can be written as:

$$I_{QRE}(\nu_Q)(\Omega, B_{ev}) = p_{QRE} \cdot p_T$$

$$= |\langle \Psi_\alpha(\Omega)|\widehat{I}_-|\Psi_\beta(\Omega)\rangle|^2 \cdot \frac{e^{(E_\alpha - E_\beta)/k_B T}}{\sum_{i,j} e^{(E_i - E_j)/k_B T}}$$

$$\bar{I}_{QRE}(\nu_Q)(B_{ev}) = \sum_\Omega \left[\frac{I_{QRE}(\nu_Q)(\Omega, B_{ev})}{1 + (\nu - \nu_Q(\Omega, B_{ev}))/\gamma} \right] \Bigg/ N$$

$$(8)$$

where the angle averaged intensity $\bar{I}_{QRE}(\nu_Q)$ is formed assuming Lorentzian peaks of constant width γ.

From the simulation's point of view, the definition of the direction of the applied evolution field B_{ev} decides whether raising operator $\widehat{I}_+$ or the lowering operator $\widehat{I}_-$ should be used. In our case, B_{ev} points into the positive z direction, which means that the proton state $|+1/2\rangle$ has lower energy and R_1-relaxation therefore is connected with an angular momentum change by $\Delta m = +1$. Therefore, the operator of choice to calculate the NQR spectra is the lowering operator $\widehat{I}_-$. However, as shown in Section 3.2, this is not a strict rule for all transitions.

2.5. The indicator function for QRE peaks

Taking together the above derived Equations (4) and (9), we are ready to write down an indicator function f_{QRE} for the potential of finding QRE peaks in a R_1-NMRD measurement of protons coupled to a QN in solids:

$$f_{QRE}(\nu_L) = \bar{I}_{QRE}(\nu_Q(B_{ev})) |_{\nu_L} \qquad (9)$$

which simply means, that the intensity of the NQR powder spectrum $\bar{I}_{QRE}$ seen by a proton ^{1}H coupled to a QN at a particular magnetic field B_{ev} is evaluated at the corresponding proton Larmor frequency ν_L.

In principle, Equation (9) can also be used to consider double quantum transitions by using $\widehat{I}_-\widehat{I}_-$ and involving two protons.

3. Results

Equation (9) is evaluated for tris(2-6-dimethoxyphenyl) bismuthine and tris(2-methoxyphenyl) bismuthine based on their NQR parameters taken from [25]. The used input parameter Q_{cc}, η, γ and the step sizes for B_{ev} and ν_Q for the calculations are summarised in Table 1. Simultaneously, the results are compared to experimental R_1-NRMD profiles which can be found in reference [2]. The molecular structure of the Bi-aryl compounds is included as an insert in Figures 4 and 5.

As already addressed in Section 2.1, the result of the QRE simulation is somewhat noisy due to the random character in the calculation of the NQR spectrum. Because of that, a post processing step is performed by smoothing the result using a moving average filter (filter parameters for coefficients see Table 1).

3.1. Tris(2-6-dimethoxyphenyl) bismuthine

The result for BiPh$_3$(DiOMe)$_3$ ortho is illustrated in Figure 4. The upper panel shows the experimental NMRD data at 295 K with many pronounced QRE peaks A–E. The positions of peaks C–E are well reproduced by the simulation according to Equation (9) (input parameters see Table 1) in the lower panel. Also, their shape (shoulder to higher frequencies) is reproduced well. For the low frequency features (<40 MHz) A and B on the contrary, no such good correspondence can be found.

3.2. Tris(2-methoxyphenyl) bismuthine

BiPh$_3$(OMe)$_3$ ortho has two crystal sites A and B with their Q_{cc} only differing by about 1 MHz and a similar η (see Table 1). Correspondingly, the NMRD profile (at 295 K) shows single peaks (A–E), where both nuclei contribute on the same frequency (within experimental accuracy). This is illustrated in Figure 5, where the lower panel shows the simulation for both sites in blue and green solid line according to Equation (9) and using the input parameters of Table 1. The locations and shapes of peaks C–E are well reproduced by the calculation. The low frequency features (<40 MHz) A and B, on the contrary, are very strong in the experiment, but are estimated weaker by the simulation. Reasons for that will be discussed in addressed in Section 4.3. Also, a frequency match is only present for feature A. Peak B has no correspondence in the simulation.

3.3. Double quantum transitions

Calculations were performed to look for double quantum transitions using the $\widehat{I}_-\widehat{I}_-$ operator and also allowing double proton transitions (crossings with $2 \cdot \nu_L$).

Figure 4. Comparison of QRE prediction calculation according to Equation (9) (lower panel) at 310 K with experimental R_1-NMRD profile of tris(2-6-dimethoxyphenyl) bismuthine (upper panel) at 295 K.
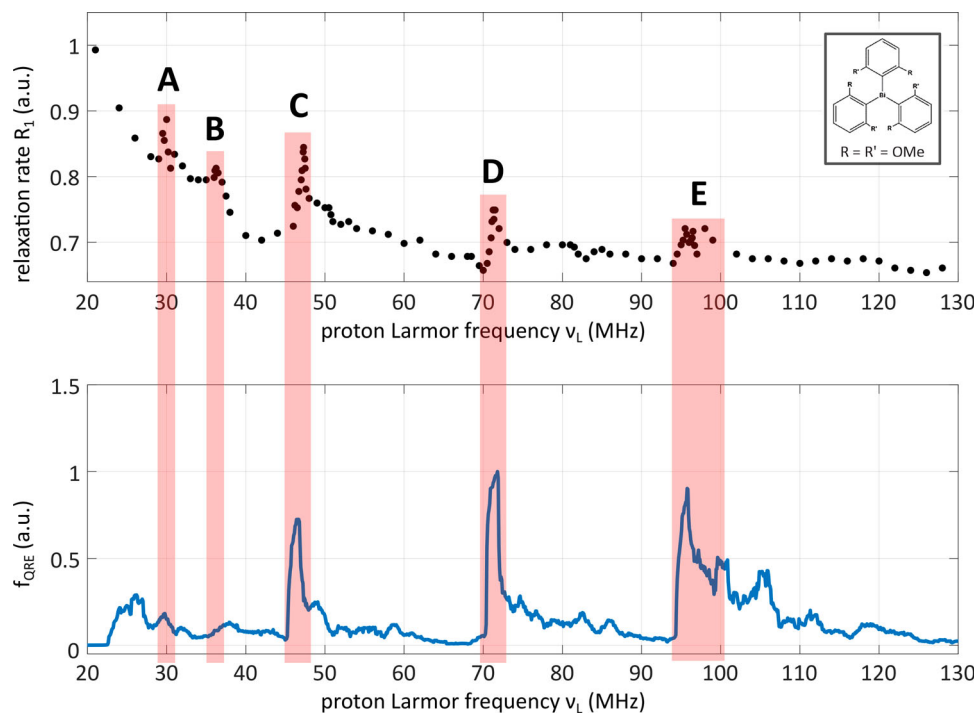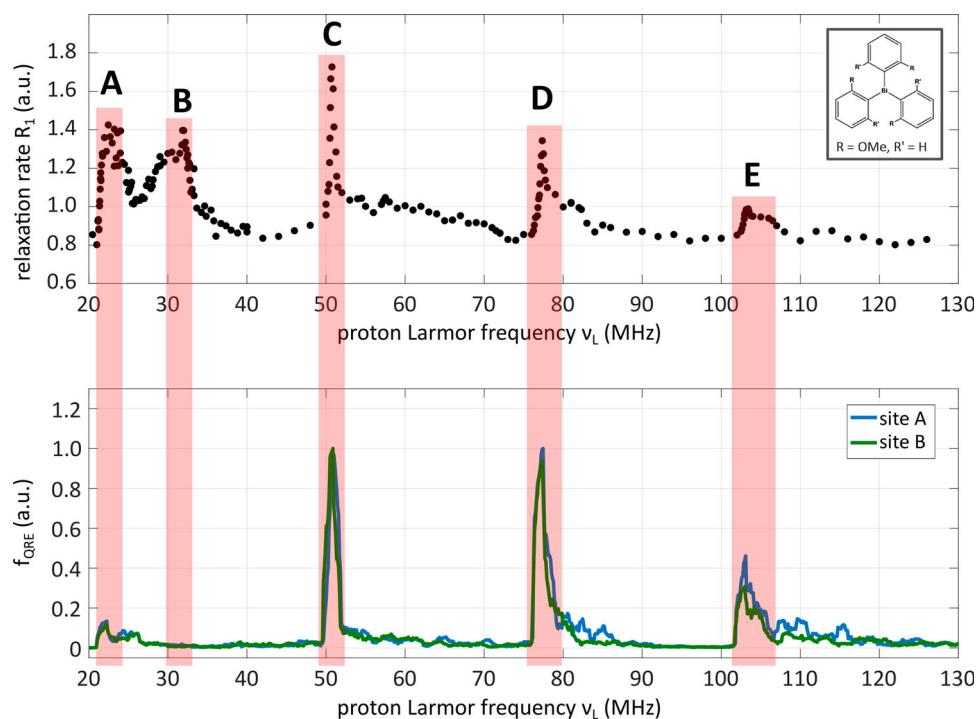

Figure 5. Comparison of QRE prediction calculation according to Equation (9) (lower panel) at 310 K with experimental R_1-NMRD profile of tris(2-methoxyphenyl) bismuthine site A and B (upper panel) at 295 K.

Equation (9) is therefore applied using $\widehat{I}_-\widehat{I}_-$ instead of $\widehat{I}_-$ and evaluated at $2 \cdot \nu_L$ with the input parameter of Table 1.

The results are shown in Figures 6 and 7, where the area of low field features is marked with a transparent vertical strip (red) in the upper panel with simulations for both cases in the lower panel. The filled solid line (blue) corresponds to the simulation using $\widehat{I}_-$, the unfilled solid line (red) to the simulation using $\widehat{I}_-\widehat{I}_-$. An overlay of both procedures suggests a slightly better match in the

Table 1. Simulation input parameters for Bi-aryl compounds tris(2-6-dimethoxyphenyl) bismuthine and tris(2-methoxyphenyl) bismuthine.

Compound	Molecular formula	Q_{cc} (MHz)	η (1)	γ (kHz)[a]	Smoothing span[b]	Step size B_{ev} (mT)	Step size ν_Q (kHz)
Tris(2-6-dimethoxyphenyl) bismuthine	$BiPh_3(DiOMe)_3$ ortho	660.9	0.105	20	11	2.1 ($\cong$88 kHz)	13.8
Tris(2-methoxyphenyl) bismuthine site A	$BiPh_3(OMe)_3$ ortho A	715.3	0	20	15	2.8 ($\cong$120 kHz)	15.4
Tris(2-methoxyphenyl) bismuthine site B	$BiPh_3(OMe)_3$ ortho B	714.2	0	20	15	2.8 ($\cong$120 kHz)	15.4

Note: NQR parameter Q_{cc}, η and linewidth $\gamma = FWHM/2$ at 310 K from reference [25].
[a] Low pass filter with coefficients equal to 1/*span* with *span* in percentage of number of data points.
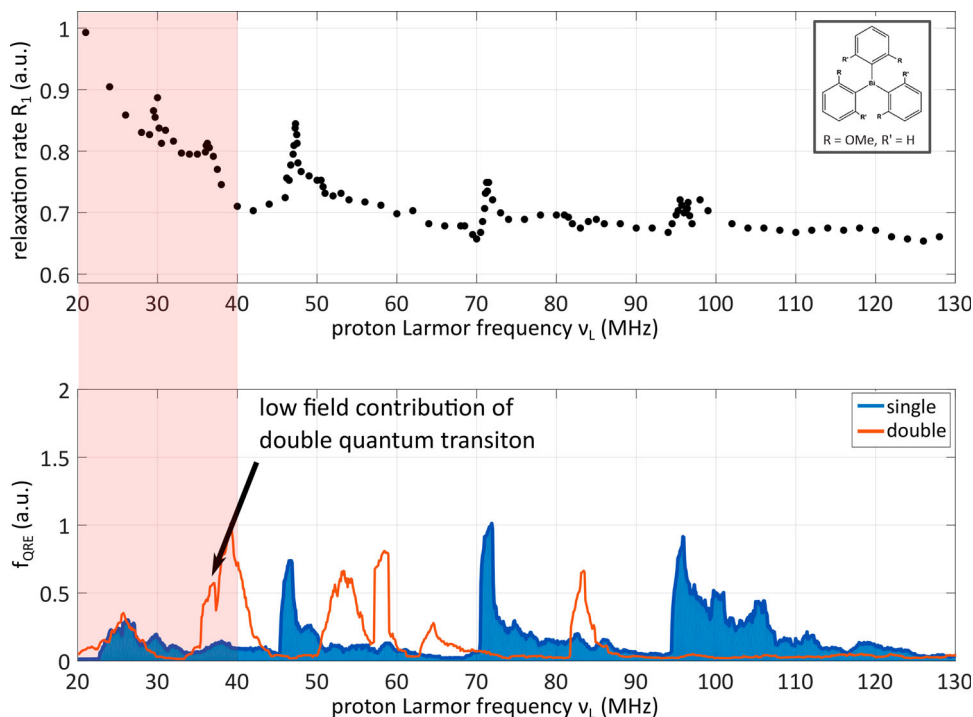[b] An average value has been assumed for all transitions.

Figure 6. Comparison of QRE prediction calculation according to Equation (9) (lower panel) at 310 K with experimental R_1-NMRD profile of tris(2-6-dimethoxyphenyl) bismuthine (upper panel) at 295 K. Lower panel: The solid line with filled area (blue) shows the calculation based on single quantum transitions. The unfilled solid line (red) shows the calculation based on double quantum transitions (Colour online, B&W in print).

low field region to the experimental data than the sole $\widehat{I_-}$ calculation.

Possible reasons for the comparably poor reproduction of the low field features and the meaning of the additional peaks in the simulation in the high field region are addressed in Section 4.

4. Discussion

The proposed procedure for predicting the appearance of QRE peaks in[1]H-NMRD profiles of the R_1 relaxation rate of molecular crystals performs well for several experimentally investigated Bi-aryl compounds in the higher field range, though a couple of assumptions have been applied. In some sense, the method represents an extension to the QRE peak allocation of a previous work [2], where rather broad frequency bands attributed to QRE locations could be defined.

4.1. The low field regime < 1 T

As the correspondence between simulation and experiment in the low field regime is not satisfactory when considering only single quantum transitions (Figures 4 and 5), also the role of possible double quantum transitions is discussed.

The low field features A and B in the NRMD profiles of the two Bi-aryl species most likely originate from the lowest NQR transitions, $|\pm 3/2\rangle$ to $|\pm 1/2\rangle$, similar to the spectrum shown in Figure 3, panel b. This is a special transition compared to higher ones, as in case of Zeeman-splitting, the corresponding Hamiltonian $\widehat{H}_0(I)(\Omega)$ (Equation (2a)) exhibits large off-diagonal elements which induce a mixing of the $|+1/2\rangle$ and $|-1/2\rangle$ states [26]. Due to that mixing, the selection rule due to the conversion of angular momentum is not restricted to $\Delta m = -1$ any
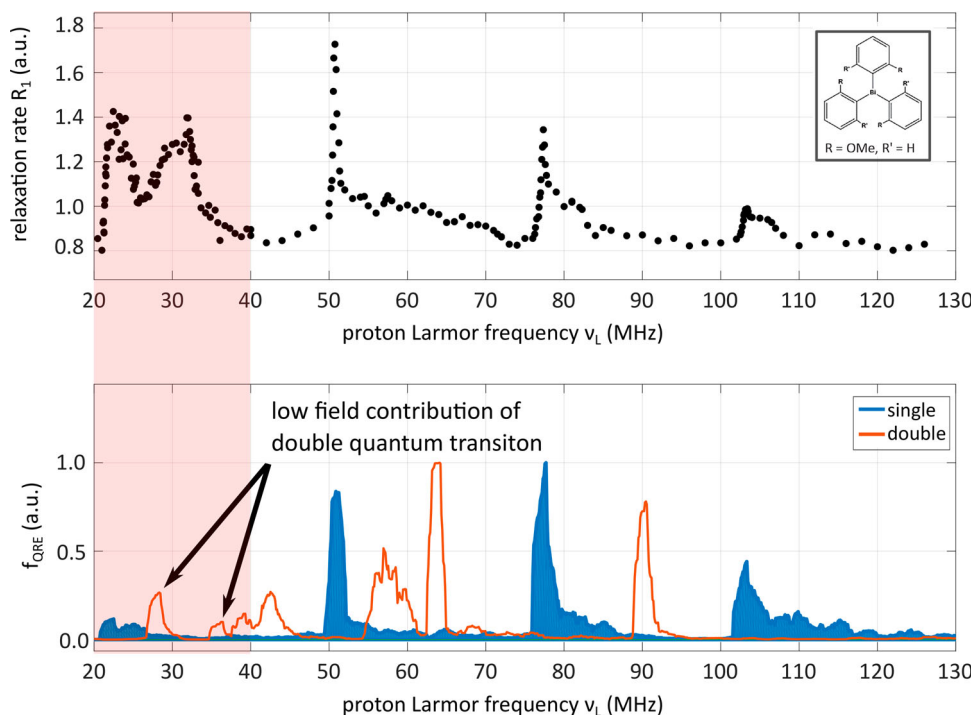
Figure 7. Comparison of QRE prediction calculation according to Equation (9) (lower panel) at 310 K with experimental R_1-NMRD profile of tris(2-methoxyphenyl) bismuthine site A (upper panel) at 295 K. Lower panel: The solid line with filled area (blue) shows the calculation based on single quantum transitions. The unfilled solid line (red) shows the calculation based on double quantum transitions (Colour online, B&W in print).

more. In that case, also double quantum transitions $\Delta m = -2$ are allowed and the simulation should also include contributions from the $\widehat{I}_-\widehat{I}_-$ operator. Also, one must take into account, that for such a transition, two protons have to be involved to maintain angular momentum.

The result when including double quantum transitions is shown in Figures 6 and 7. The data suggest that double quantum transitions can contribute to QRE in the frequency range/field range associated with the lowest NQR transition.

4.2. The high field regime > 1 T

QRE peaks occurring at $\nu_L > 40$ MHz can be predicted well both in location and shape by assuming only single quantum transition. This is demonstrated in Figures 4 and 5.

The slight mismatch in frequency (down-shifted simulation) can be attributed to the temperature difference (simulation at 310 K, experiment at 295 K) and experimental errors both in the R_1-NMRD profile and in the used NQR parameter for the simulation. As has been shown in [25], the temperature coefficient of NQR transitions around 310 K is expected about 10 kHz/K, at worst. For an assumed temperature difference of about 20 K, this means one can expect a shift of 0.2 MHz for the

QRE peaks, which is of the order of the experimental resolution.

However, the exact relative intensities of the QRE features and the baseline shape due to a relaxation background cannot be reproduced. This is not surprising as corresponding models have not yet been included.

The additional peaks at higher frequencies from the simulation of double quantum transitions (red lines in Figures 6 and 7) do not originate from such special conditions as addressed above and are thus also not observed in the experiment (as such transitions are forbidden). Although, in principle also these higher states are subjected to a mixing due to non-zero η and the angle dependency of the Zeeman Hamiltonian, this effect is significantly lower than for the lowest transition. Therefore, corresponding features cannot be observed in the experiment.

4.3. Possible improvements

Most worth mentioning is the fact that the actual D–D coupling mechanism between QNs and protons has not been included into the formulation. Also, no other relaxation mechanism, as e.g. the proton D–D background, has been considered. The method is solely based on the probability of the QN NQR transitions which are available for the QRE effect.

One attempt to include relaxation processes could be a model based on D–D coupling between heterogeneous nuclei extended by a suitable model for the quadrupolar spin fluctuations. This could increase the accuracy of the simulation of predicting also the exact intensities of possible QRE features, which are not perfectly reproduced by the current method. Also, a model for the proton relaxation background based on dipolar coupling could be used to add a more realistic baseline to the presented calculations.

In particular, a high spectral density at the matching frequency enabling efficient QRE can be responsible for the strong mismatch in predicting the relative QRE peak intensities (see Figure 4 and 5) between low field and high field QRE peaks.

The next step would be to consider the whole spin system and all relaxation effects directly in a Redfield theory [10] approach, which is considerably more complex and requires more computational resources.

Another point for improvement is the calculation of the static NQR powder spectrum depending on an external magnetic field. Instead of assuming a constant width for all transitions, a proper model based on Redfield theory can be applied to calculate the lineshape throughout the whole spectrum. In that way, the actual peak widths, which are different for each transition, could be included which would certainly better resolve the experimentally observed QRE peak shape.

4.4. Conclusion

The comparison between experiment and simulation is satisfactory in the high field region ($> 1\,\mathrm{T}$) and so the presented method can be used to plan R_1-NMRD measurements in advance by predicting QRE peak positions in QN and ^{1}H containing molecular crystals. The necessary NQR parameters Q_{cc}, η and the linewidth can be determined either experimentally from NQRS measurements or by ab *initio* QC calculations as already has been shown to give reasonable results [25].

As the actual relaxation effect between ^{1}Hs and QNs is not included, the procedure does not provide quantitative information and shall therefore be treated as a prediction tool for frequencies where QRE peaks are likely to occur. More precisely, the presented procedure shows at which field strengths there is no or little chance for a QRE peak and so states a necessary condition that can serve as a basis for further considerations.

When it comes to an application of the presented method, we would like to mention that the tool can support ongoing research on MRI contrast agents based on the QRE effect [2, 15, 25] which is especially suitable for FFC-MRI systems [24]. Of course, the requirements and

conditions for a particle acting as MRI contrast agent in biological tissue are rather complex and not straightforward to fulfil. However, in a rational particle design process, it makes sense to start with the simplest system and extracting promising compound candidates already from the solid state. By doing so, to some degree the frequency (magnetic field) positions where the QRE effect most likely occurs can already be restricted. In a next step, the selected particles can be brought into solution (water) by, e.g. incorporating them in a nano particle acting as blood stream carrier. For this overall particle system further properties, as e.g. water exchange, rotational dynamics and solubility have to be shaped. This topics are matter of ongoing work where further research is desirable. In a quite recent work, aspects of structural order of QRE-active particles based on ^{209}Bi are discussed with the outcome, that also in solution, particles with a highly ordered molecular structure are beneficial [29].

ORCID

Christian Gösweiner http://orcid.org/0000-0003-4453-9385
Danuta Kruk http://orcid.org/0000-0003-3083-9395

References

[1] F. Fujara, D. Kruk, and A.F. Privalov, Prog. Nucl. Magn. Reson. Spectrosc. **82**, 39–69 (2014).
[2] D. Kruk, E. Umut, E. Masiewicz, C. Sampl, R. Fischer, S. Spirk, C. Goesweiner, and H. Scharfetter, Phys. Chem. Chem. Phys. **20** (18), 12710–12718 (2018).
[3] F. Noack, Prog. Nucl. Magn. Reson. Spectrosc. **18** (3), 171–276 (1986).
[4] O. Lips, D. Kruk, A. Privalov, and F. Fujara, Solid. State. Nucl. Magn. Reson. **31** (3), 141–152 (2007).
[5] F. Bonetto, E. Anoardo, and R. Kimmich, J. Chem. Phys. **118** (19), 9037–9043 (2003).
[6] E. Rommel and F. Noack, J. Phys. Chem. **92** (10), 2981–2987 (1988).
[7] N. Fatkullin, R. Kimmich, and H.W. Weber, Phys. Rev. E **47** (6), 4600–4603 (1993).
[8] S. Stapf, R. Kimmich, R.O. Seitter, A.I. Maklakov, and V.D. Skirda, Colloids Surf. A: Physicochem. Eng. Aspects **115** (15), 107–114 (1996).
[9] R. Kimmich, E. Anoardo, Prog. Nucl. Magn. Reson. Spectrosc. **44** (3-4), 257–320 (2004).
[10] A.G. Redfield, Adv. Magn. Opt. Reson. **1** (C), 1–32 (1965).

[11] D.E. Woessner and H.S. Gutowsky, J. Chem. Phys. **29** (4), 804 (1958).

[12] G. Voigt and R. Kimmich, J. Magn. Reson. (1969) **24** (1), 149–154 (1976).

[13] P.O. Westlund and H. Wennerstrom, J. Magn. Reson. **63** (2), 280–286 (1985).

[14] P.O. Westlund, Phys. Chem. Chem. Phys. **12** (13), 3136–3140 (2010).

[15] D. Kruk, A. Kubica, W. Masierak, A.F. Privalov, M. Wojciechowski, and W. Medycki, Solid. State. Nucl. Magn. Reson. **40** (3), 114–120 (2011).

[16] D. Kruk, J. Altmann, F. Fitfara, A. Gädke, M. Nolte, and A.F. Privalov, J. Phys. Condens. Matter **17** (3), 519–533 (2005).

[17] M. Nolte, A. Privalov, J. Altmann, V. Anferov, and F. Fujara, J.Phys. D, Appl. Phys. **35** (9), 939–942 (2002).

[18] R. Kimmich, W. Nusser, and F. Winter, Plasma Sources Sci. Technol. **29** (5), 593–596 (1984).

[19] R. Kimmich, F. Winter, W. Nusser, and K.H. Spohn, J. Magn. Reson. (1969) **68** (2), 263–282 (1986).

[20] D.J. Lurie, S. Aime, S. Baroni, N.A. Booth, L.M. Broche, C.H. Choi, G.R. Davies, S. Ismail, D. Ó hÓgáin, and K.J. Pine, CR Phys. **11** (2), 136–148 (2010).

[21] E.S. Lee, L. de Rochefort, G. Ferrante, and B.K. Rutt, Proc. Intl. Soc. Mag. Reson. Med. **20**, 2877 (2012).

[22] U.C. Hoelscher, S. Lother, F. Fidler, M. Blaimer, and P. Jakob, Magn. Reson. Mater. Phys., Biol. Med. **25** (3), 223–231 (2012).

[23] C.T. Harris, W.B. Handler, Y. Araya, F. Martinez-Santiesteban, J.K. Alford, B. Dalrymple, F. Van Sas, B.A. Chronik, and T.J. Scholl, Magn. Reson. Med. **72** (4), 1182–1190 (2014).

[24] M. Bödenler, M. Basini, M. Francesca Casula, E. Umut, C. Gösweiner, A. Petrovic, D. Kruk, and H. Scharfetter, J. Magn. Reson. **290**, 68–75 (2018).

[25] C. Gösweiner, P. Lantto, R. Fischer, C. Sampl, E. Umut, P.O. Westlund, D. Kruk, M. Bödenler, S. Spirk, A. Petrovič, and H. Scharfetter, Phys. Rev. X **8** (2), 021076 (2018).

[26] T.P. Das and E.L. Hahn, in *Nuclear quadrupole resonance spectroscopy* Solid state physics. Supplement 1 (Academic Press, New York, 1958), pp. ix, 223 p.

[27] C.P. Slichter, in *Principles of Magnetic Resonance*, Springer Series in Solid-State Sciences, Vol. 1 (Springer, Berlin Heidelberg, Berlin, Heidelberg, 1990), p. 658.

[28] D. Possa, A.C. Gaudio, and J.C.C. Freitas, J. Magn. Reson. **209** (2), 250–260 (2011).

[29] H. Scharfetter, C. Gösweiner, P.J. Krassnig, C. Sampl, M. Thonhofer, R. Fischer, S. Spirk, R. Kargl, K. Stana-Kleinschek, E. Umut, and D. Kruk, Mol. Phys. **8976**, 1–9 (2018).